Structure of the hexagonal phase of the sodium dodecyl sulfate and water system

R. Itri and L. Q. Amaral
Instituto de Física, Universidade de São Paulo, Caixa Postal 66318, 05389-970 São Paulo, São Paulo, Brazil

P. Mariani
Istituto di Scienze Fisiche, Università di Ancona, I-60131 Ancona, Italy
and Research Unit of INFM, Istituto Nazionale per la Fisica Della Materia, Ancona, Italy
(Received 10 May 1996)

The hexagonal cell parameter a of the system sodium dodecyl sulfate and water in the H_α phase as a function of volume concentration c_ν presents the functional behavior expected for rigid and finite objects: $a \propto c_\nu^{-1/3}$. The micellar particle length is, however, unknown since its derivation depends intrinsically on the particle radius R considered. A constant radius is found for the whole H_α domain, and the electron density maps obtained from the x-ray diffracted intensities are analyzed and allow determination of micellar radius (effective radius $R_{\rm eff}=18.4\pm0.1$ Å, paraffin radius $R_{\rm par}=16.7\pm0.1$ Å, and total radius $R_{\rm tot}=20.5\pm1.0$ Å). From these values the resulting micellar size is between 170 and 640 Å, with a value of 260 Å for $R_{\rm tot}=20.5$ Å. [S1063-651X(96)06411-2]

PACS number(s): 61.30.Eb, 83.70.Jr

I. INTRODUCTION

The structure of the lyotropic hexagonal H_α phase (α means the disordered paraffin chain) has been assumed since the initial works to consist of ''infinite'' cylindrical micelles, with a two-dimensional hexagonal positional order in the plane perpendicular to the cylinder axes [1,2]. A functional behavior $a \propto \nu_p^{-1/2}$ (a, hexagonal unit cell parameter; ν_p, particle volume fraction) is expected for ''infinite'' or flexible objects when the packing is essentially end to end and compression only occurs in the lateral directions as ν_p increases [3]. Such behavior has been observed, for instance, in an H phase following a cholesteric phase (N^*) [4]. A study of a sodium dodecyl sulfate (SLS)–water system [5] at 70 °C, which presents an isotropic (I)-H_α transition, shows, however, a functional behavior $a \propto \nu_p^{-1/3}$, typical of compression in all three dimensions, leading to the idea that finite hard rods [6] are present in the H_α domain.

Recent statistical mechanics theories for systems with self-assembly have been able to predict the occurrence of a direct $I-H_\alpha$ transition and the conditions for appearance of an intermediate nematic (N) phase both in polydisperse finite-rigid rods [7] and ''infinite''-flexible [3] polymers. The polydispersity of the rod lengths is a necessary condition for suppression of a smectic phase between I and H_α phases [8]. Such polydispersity could be responsible for the lack of detectable out-of-plane scattering in the H phase, which was one of the hindrances to accepting the hypothesis of finite rods in the H domain. The self-assembly properties imply the possibility of growth of the rods in all the phases. It has also been recently shown that $a \propto \nu_p^{-x}$ with $x<1/3$ could characterize micellar growth with concentration in the hexagonal domain [9,10].

What now starts to become clear from the experimental work in H phases [4,5,9–12] is that the exponent x may provide evidence for H phases with different structural characteristics that are correlated with the specific neighboring phases and phase transitions. Some experimental results, like the observation of very short rods in the hexagonal phases of guanosine derivatives and analogs [11] or the visualization in lipid hexagonal phases of very long rods by electron microscopy, should be taken in relation to the particular investigated system, and should not be generalized as characteristic of all H phases. Furthermore, the basic properties of growth and flexibility should not be necessarily associated with rigid rods [7] and polymers [3], respectively. Rigidity-flexibility of the rods could also define $\frac{1}{3}$ and $\frac{1}{2}$ behavior even in nonpolymeric systems.

In this paper a more detailed analysis of the results in the H_α phase of the SLS-water system is presented.

The isotropic I phases of the SLS-water system at 25 °C were studied by x-ray scattering from low concentrations [13,14] up to concentrated solutions close to I-H_α phase transition [12,15,16]. The detailed small angle x-ray data analysis focusing on micellar growth in the vicinity of the isotropic I to liquid crystalline phase transition demonstrated that micelles are small and they grow little in the I phase (anisometry around 2.4–3 near $I \rightarrow H_\alpha$) [15,16].

The micellar particle length L is unknown in the H_α phase and its determination from x-ray results in the hexagonal phase depends intrinsically on the particle radius R considered [5]. In the previous work [5] the imprecision of the R value precluded the inference of L from the measured values of the cell parameter. This paper discusses in more detail the R values for the SLS-water system, taking into account the electron density maps obtained from the analysis of the x-ray diffracted intensities.

II. EXPERIMENT

Commercial Sigma SLS (99% purity) and bidistilled water were mixed in different amounts (SLS ranging from 37.8 up to 62 wt %) and investigated by using an x-ray generator equipped with a Guinier-type focusing camera with a bent quartz monochromator. The samples were mounted in vacuum-tight cells with thin mica windows; the cells were

continuously rotated during the exposure in order to reduce spottiness. Measurements were taken at 70 °C [5]. The films were microdensitometered and the intensities measured as reported in Ref. [17] ($s=2\sin\theta/\lambda$; 2θ is the scattering angle; λ is the Cu $K\alpha$ x-ray wavelength).

III. ANALYSIS METHOD

A. X-ray diagrams

Four reflections with a typical spacing ratio $1:\sqrt{3}:\sqrt{4}:\sqrt{7}$ were usually present, compatible with a two-dimensional hexagonal lattice of $p6m$ symmetry. The unit cell parameter a is given by

$$a=\frac{2}{\sqrt{3}}\frac{\sqrt{h^2+k^2+hk}}{s(hk)},$$

where h and k are the Miller indices of the reflections and $s(hk)$ is the peak position in the reciprocal space (Å^{-1}). No scattering in the direction perpendicular to the hexagonal plane was observed: under the hypothesis that finite rods are present in the hexagonal phase, this fact shall be ascribed to polydispersity of cylinder length which is a necessary condition for the occurrence of a direct isotropic-hexagonal phase transition [7,8].

B. Hexagonal phase model

By assuming that finite cylinders with radius R and average length L are packed as a fluid in the third dimension (normal to the hexagonal plane) with an average distance C between particle centers, the following equation can be written [5–9]:

$$\pi R^2(L/C)=\sqrt{3}a^2\nu_p/2, \tag{1}$$

where ν_p is the particle volume fraction.

In the case of micelles, care must be taken in the definition of the ''particle.'' Assuming that practically all monomers are incorporated in the micellar aggregate, it is possible to consider $\nu_p=c_\nu$ (amphiphile volume concentration). In such a case the values R and L in Eq. (1) should refer to ''effective'' values R_{eff} and L_{eff} that represent the ''particle without water.'' Alternatively, $\nu_p=c_{\nu\text{par}}$ (volume concentration of the paraffin moiety) and values in Eq. (1) are R_{par} and L_{par}. For a cylinder it is possible to write $L_{\text{par}}=L_{\text{eff}}$. As a consequence, there is a necessary relation between these micellar radii:

$$R_{\text{eff}}/R_{\text{par}}=\sqrt{c_\nu/c_{\nu\text{par}}}. \tag{2}$$

For long-flexible rods, the relation $L/C=1$ leads to the $a\propto\nu_p^{-1/2}$ behavior. For finite-rigid rods the assumption of uniform decrease in interparticle distances in all three dimensions is equivalent to the relation [5,9]

$$L/C=2R/a. \tag{3}$$

It shall be stressed that this relation refers to the ''total particle,'' which may contain bound water. Therefore in Eq. (3) the values are R_{tot} and L_{tot}. For a cylinder it is possible to assume $L_{\text{tot}}=L_{\text{eff}}=L_{\text{par}}$, leading to

$$a=2R(2\sqrt{3}/\pi)^{-1/3}\nu_p^{-1/3} \tag{4}$$

corresponding to the $a\propto\nu_p^{-1/3}$ behavior.

Considering the pairs $(R_{\text{par}},c_{\nu\text{par}})$ or (R_{eff},c_ν) Eq. (4) is replaced by

$$R_{\text{eff}}^2R_{\text{tot}}=\frac{\sqrt{3}}{4\pi}a^3c_\nu. \tag{5}$$

In the case of finite micelles it may be important to consider a more realistic model of spherocylinders, with $L=\ell+2R$ and anisometry $\mu=\ell/2R$. Modifying Eq. (1) accordingly leads to

$$\pi R^2\ell+\frac{4}{3}\pi R^3=\frac{\sqrt{3}}{2}Ca^2\nu_p. \tag{6}$$

Equation (3) is kept for the case of spherocylinders, since it expresses a condition related to the center of mass of the oriented particles, leading to [5,9]

$$a=2R\left[\frac{\pi}{2\sqrt{3}}\frac{\mu+2/3}{\mu+1}\right]^{1/3}\nu_p^{-1/3}. \tag{7}$$

Developing the equations it results that, in Eq. (7), in the numerator one should have $(R_{\text{eff}},\mu_{\text{eff}},c_\nu)$ or $(R_{\text{par}},\mu_{\text{par}},c_{\nu\text{par}})$, with μ_{tot} in the denominator. The conditions for existence of a solution in such cases for Eq. (7) are

$$R_{\text{eff}}^2R_{\text{tot}}\geqslant\frac{\sqrt{3}}{4\pi}a^3c_\nu,\quad (R_{\text{eff}})^3\leqslant\left(\frac{3}{2}\right)\frac{\sqrt{3}}{4\pi}a^3c_\nu \tag{8}$$

corresponding, respectively, to L values decreasing from ∞ to $2R$ (spherical micelles).

In the case of spherocylinders the use of Eq. (7) for the pairs (R_{eff},c_ν) and $(R_{\text{par}},c_{\nu\text{par}})$ leads to the relation

$$\left(\frac{R_{\text{eff}}}{R_{\text{par}}}\right)^3=\frac{c_\nu}{c_{\nu\text{par}}}\frac{\mu_{\text{par}}+2/3}{\mu_{\text{eff}}+2/3}. \tag{9}$$

It should be stressed that the information regarding the micellar length is lost for cylinders in Eq. (4) but it is recovered for spherocylinders in Eq. (7). This occurs because the difference in volume between a cylinder and a spherocylinder of length L is filled with water, so that the total amount of water in the direction perpendicular to the hexagonal plane now depends on the number of spherocylinders, and not only on the ratio L/C.

From the observed curve $a\propto\nu_p^{-1/3}$ one could get in principle the R value from Eq. (4) for cylinders or very long spherocylinders, or the μ value from Eq. (7) if R is known. In practice the μ value is critically dependent on the R value adopted, which precludes inference of μ from the measured hexagonal lattice parameter when R is not known with precision [5].

In cases where $a\propto\nu_p^{-x}$, with $x<1/3$, Eq. (7) gives a law for the growth of the spherocylinders with concentration [9], if R is known.

C. Electron density maps

In order to obtain more structural information about the hexagonal plane, particularly in the case of micelles where R is not known with precision, the analysis of the x-ray data may be extended to the intensity of reflections.

X-ray diffraction patterns give a set of integral intensities from which the moduli of the structure factors can be calculated as

$$|F(h,k)| = [I(h,k)/m(h,k)]^{1/2}, \tag{10}$$

where $I(h,k)$ is the intensity observed for the reflection with h,k indices and $m(h,k)$ is its multiplicity. As the structure is center symmetric, each amplitude has a phase angle ϕ equal to 0 or π, i.e., each amplitude can be positive or negative. Then the phase problem is reduced to the sign problem. In lipid crystallography this problem can be solved by performing swelling experiments: the unit cell dependence on the water concentration allows one to sample the continuous structure function. Then, the signs of each structure factor may be deduced observing the behavior close to the zeros of intensities [18]. As usual [19] the intensities of all reflections observed in any experiment of the swelling series are reduced to $I(h,k)/\Sigma_{h,k} I(h,k)$ and then normalized so that

$$\sum_{h,k} I(h,k) = \sigma/\sigma_{\min}, \tag{11}$$

where σ and $\sigma_{\min}$ are the unit cell surfaces of each sample and of the smallest cell dimension in the series.

After the $F(h,k)$ signs are chosen, the electron density distribution is computed by Fourier transform, by using $F(h,k)$ values obtained from the experimental intensities [Eq. (10)]. According to Ref. [20] the normalization $\Sigma_{h,k} I(h,k) = 1$ was used, a procedure which leads to dimensionless expressions for both structure factors and is called the ''electron density map,'' in short ''map,'' where $\langle\rho\rangle$ is the average value of $\rho(x,y)$ over the surface of the unit cell,

$$\Delta\rho = [\rho - \langle\rho\rangle]/[\rho^2 - \langle\rho^2\rangle]^{1/2}.$$

There is here a point to be discussed, since in the case of finite rods the procedure gives in fact a two-dimensional (2D) projection in the hexagonal plane of a 3D electron density map. The only difference between the projection and the section is that the average level $\langle\rho\rangle$ of the projection corresponds to a weighed average between the $\langle\rho\rangle$ of the section and the ρ_0 of water, weighed according to L and $(C\text{-}L)$. In fact, if the values $\langle\rho\rangle$ and ρ_0 were sufficiently different, this could be an independent method to determine the cylinder length L. However, the fact that $\langle\rho\rangle$ and ρ_0 are very close to each other makes impossible the determination of L from the normalization procedure. But it is clear that it is possible to analyze the structure of the projection, as long as one is careful to note that the $\langle\rho\rangle$ value has no absolute meaning.

Some electron density maps will be shown in this paper: they are represented using equally spaced density levels. Negative levels (which correspond to the low-electron-density regions in relation to $\langle\rho\rangle$ considered as arbitrary zero level in the 2D projection) are reported as dashed lines and include the paraffinic moiety (ρ_{par}). The zero level is drawn by a full line as well as the high-electron-density levels. These levels include the polar region (head groups and hydration water) ρ_{pol}.

TABLE I. SLS concentration (in wt %), the corresponding volume fraction c_ν (calculated by using 0.92 and 1.034 g/cm^3 for SLS and water specific volumes, respectively, at 70 °C), and corresponding unit hexagonal cell parameter a.

c (wt %)	c_ν	a ($\pm$1.0 Å)
37.8	0.351	51.0
38.0	0.353	50.9
40.0	0.372	49.6
41.0	0.382	49.0
45.0	0.421	48.4
48.0	0.451	46.6
52.0	0.491	45.6
55.0	0.521	44.6
57.0	0.541	44.3
58.0	0.551	43.8
62.0	0.592	43.3

IV. RESULTS AND DISCUSSION

The a values measured as a function of SLS concentration in the H_α phase at 70 °C are given in Table I. The corresponding figure has already been published [5]. The experimental data are well fitted by the curve

$$a = 35.93(c_\nu)^{-1/3} \tag{12}$$

considering $c_\nu = 1.22 c_{\nu\text{par}}$, where $c_{\nu\,\text{par}}$ is the volume concentration of the paraffin moiety and c_ν refers to the whole amphiphile molecule (including counterions but excluding all water).

The experimental result of Eq. (12) shows that SLS micelles behave as ''finite-rigid'' particles regarding water distribution in the three dimensions. It should be noted that an exponent smaller than 1/3 should be associated with micellar growth [9], while an exponent larger than 1/3 should be associated with flexibility [3]; hence it is possible that the exponent 1/3 might correlate with a very particular combination of growth with flexibility, giving as a result a finite-rigid behavior, with a constant ''effective length.''

Equation (12) together with (7) imply defined conditions for the micellar radius and anisometry:

$$R_{\text{eff}}\left(\frac{\mu_{\text{eff}} + 2/3}{\mu_{\text{tot}} + 1}\right)^{1/3} = 18.6 \text{ Å}, \tag{13}$$

with $R_{\text{eff}} \leqslant 21.3$ Å and $R_{\text{eff}}^2 R_{\text{tot}} \geqslant (18.6)^3$ Å.

To give a better idea of the precision of the assumption made in Eq. (3), the values obtained from Eq. (7) and the original data of Table I are given in Fig. 1. The fact that $R_{\text{eff}}[(\mu_{\text{eff}} + 2/3)/(\mu_{\text{tot}} + 1)]^{1/3}$ remains constant in the whole H domain assures the validity of Eq. (3) and therefore the $a \propto c_\nu^{-1/3}$ behavior.

A delicate point in the interpretation of the results refers to the various micellar radii (R_{par}, R_{eff}, and R_{tot}). The actual

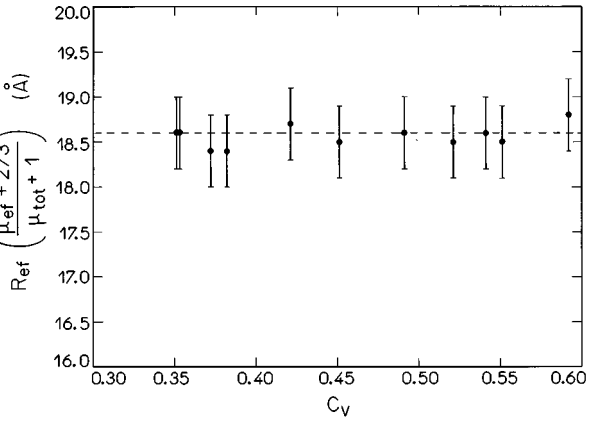

FIG. 1. $R_{\rm eff}[(\mu_{\rm eff}+2/3)/(\mu_{\rm tot}+1)]^{1/3}$ as a function of amphiphile volume concentration c_v, obtained from Eq. (7) and Table I. A constant value 18.6±0.1 Å is found for the whole H_α domain.

amount of water bound to the micelle is unknown and the polar head region (~4.6 Å thick [21]) must contain some bound water.

The electron density maps obtained from diffracted intensities will be analyzed in order to determine the actual value of the micellar radii.

The experimental values of the moduli of the structure factors [Eq. (10)] from the swelling experiments are plotted in Fig. 2. A cylindrical structure function that assumes a two-step radial electron density distribution in relation to the solvent (an inner paraffinic region with $\rho_{\rm par}$ and an outer shell with $\rho_{\rm pol}$) presents some zeros of intensities whose positions depend intrinsically on paraffinic radius $R_{\rm par}$ and electron density contrast [15,22,23]. An example of the cross-section cylindrical structure factor for the SLS system was given in a previous paper [15]. From that curve a first zero for $s<0.015$ Å^{-1} and the second one between 0.04 and 0.05 Å^{-1} are observed. A new zero of intensity appears for $s=0.07$ Å^{-1}. Based on such a model it is possible to conclude that $F(1,0)$ and $F(1,1)$ reflections in Fig. 2 have the same sign, while $F(2,1)$ has the opposite sign. The main problem remains over the choice of the sign of the $F(2,0)$ reflection, since it is located in the region of an inversion point. It seems, from Fig. 2, that even if the graph does not represent the continuous structure factor, it appears to indicate that the functions drops to zero near $s=0.05$ Å^{-1}.

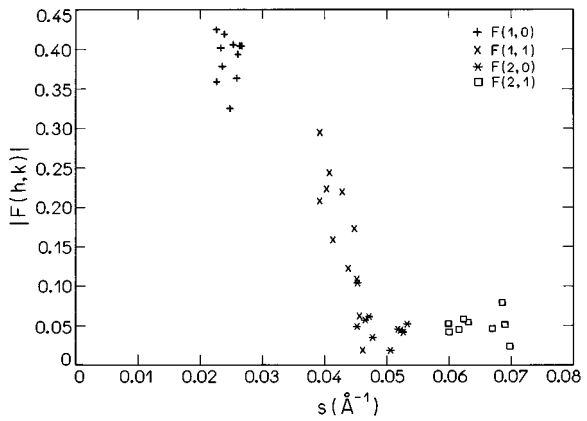

FIG. 2. Results of swelling experiments: $|F(h,k)|$ [Eq. (10)] as a function of x-ray diffraction positions [s(Å^{-1})]. $F(2,1)$ is absent for $c=48$ and 62 wt %, while $F(2,0)$ is not considered for $c=48$ wt % of SLS.

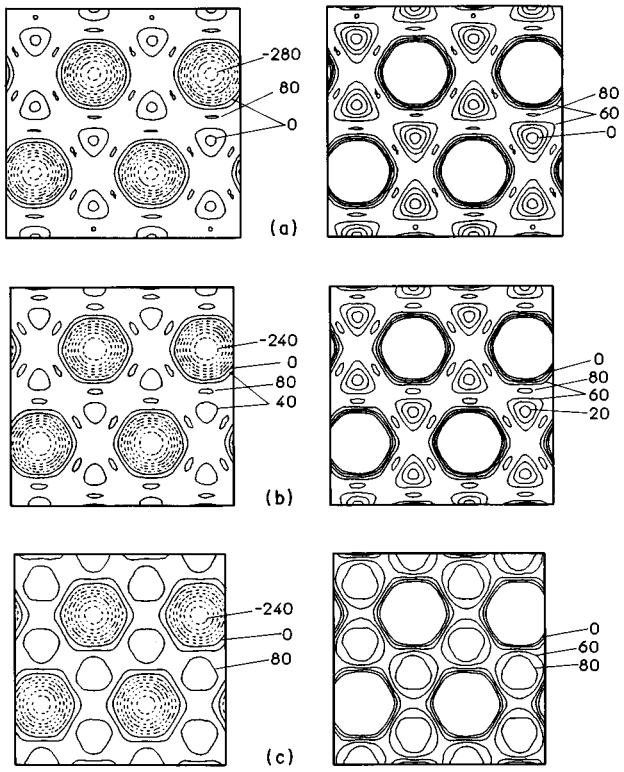

FIG. 3. Electron density distribution of the hexagonal phases of the SLS-water system at 70 °C with ϕ set $(---+)$ for all concentrations. The electron density scale is arbitrary. The intensity data have been normalized so that $\Sigma_{h,k}I(h,k)=1$. $\langle\rho\rangle$ level corresponds to an arbitrary zero level. The minimum and maximum of electron density for (a) 37.8 wt % are $\rho_{\rm min}=-294$, $\rho_{\rm max}=83$; (b) 45 wt %, $\rho_{\rm min}=-270$, $\rho_{\rm max}=84$; and (c) 58 wt %, $\rho_{\rm min}=-265$, $\rho_{\rm max}=93$, respectively. On the right side the density lines are equally spaced with an increment of 40, while on the left side the increment is 20.

Under such assumption, the sign combination $---+$ for the four observed reflections seems to be valid for samples with concentration $c<48$ wt %, while the ϕ-set combination $--++$ is valid for $c>48$%. Alternatively, the sign combination $---+$ for the whole investigated concentration range would be possible, if the zero is located around $s=0.055$ Å^{-1}.

Some of the corresponding electron density maps related to the chosen sign combinations are reported in Figs. 3 and 4 and are described below. In both figures, in the left side, the density levels have an increment of 40, while in the right side, only outer regions are represented in more detail, with density levels spaced with an increment of 20; some levels are quoted just to clear the figures, in order to emphasize the increasing-decreasing electron density level sequence.

Figures 3(a)–3(c) show some electron density maps calculated by using the $---+$ sign combination. It is evident that the maps show a similar aspect at all the studied concentrations: circular cylinder cross section in the hexagonal plane, with a negative (with respect to the average electron density value $\langle\rho\rangle$) inner region, clearly associated with the

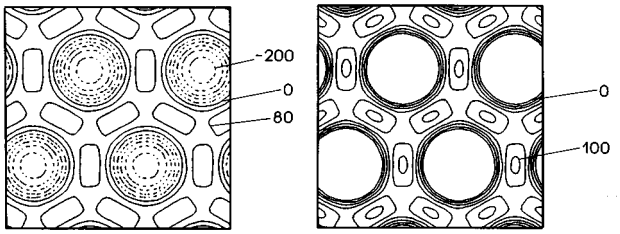

FIG. 4. ϕ set $(--++)$: 58 wt %, $\rho_{min}=-233$, $\rho_{max}=103$.

low-electron-density paraffinic medium, and an outer region with positive levels (with respect to the $\langle\rho\rangle$) which could be associated to the more dense polar moiety. In particular, the inner region is characterized by a smooth variation of electron density until about 5 Å, which can give evidence of localization of CH_3 groups ($\rho_{par}=0.167\ e/Å^3$) in the micellar center. A rapid change of the electron density values after that is therefore observed until the $\langle\rho\rangle$ level with radius around 14 Å is reached. The inner electron density distribution in isotropic diluted systems presented the same profile [14].

An increasing of the electron density values from the $\langle\rho\rangle$ level keeping a continuous contour is observed, until the distance R of 18.4 Å from micellar center is reached. This increase of the electron density value can be easily associated with the presence of the head groups. Furthermore, the maximum value of electron density is located at about 19.0 Å from the micellar center, as indicated by small islands at level 80 in the maps (a) and (b) for concentrations up to 45 wt %. In the maps reported in Figs. 3(a) and 3(b), the density minima (level 20, right side) in the polar region could be associated with the water molecules which fill the regions far away from the cylinder surface. The maps corresponding to the higher concentrations [Fig. 3(c) shows one example] do not show such decreasing of electron density value, indicating that the sign combination is incorrect.

Figure 4 shows the electron density map obtained from the 58 wt % of SLS sample by using the $--++$ sign combination. For such choice of signs, the minimum of electron density in the inner region is not so deep as for the one obtained previously, although the map still presents a smooth variation of ρ_{par} until around 5.5 Å and a faster variation until a radius of 14.5 Å is reached. The higher-density levels are closed around the paraffinic moiety until the same previous value $R=18.4$ Å is found. The main difference between this electron density map and the one presented in Fig. 3(c) is the distribution of the maxima of electron density, which are located in the mean distance between the cylinders along the parallelogram axis (around 21–22 Å from the center of the micelle). It means that the distance related to the highest levels is about 13% larger than that found for the previous sign combination chosen: considering the experimental low resolution, this fact should depend on the closeness of the cylinders. Moreover, a decreasing of electron density values in the regions far away from the cylinder surface is by contrast observed. With reference to the electron density distributions reported in Figs. 3(a) and 3(b), this map could be considered satisfactory.

As a result, it is possible to conclude that in all the maps analyzed the electron density values increase from the $\langle\rho\rangle$ level keeping a continuous contour until a constant distance of 18.4 Å from the micellar center is reached. The maxima of the electron density occur already in a discontinuous way, typically at distances of 19 Å.

A consistent interpretation of the structure is obtained by estimating R_{eff} from the electron density maps using as a criterion the largest distance of continuous contour. This leads to $R_{eff}=18.4$ Å and $R_{par}=16.7$ Å (which is precisely the length of the extended chain), with precision ± 0.1 Å. Interpreting the maximum electron density as associated with the position of the sulfur atoms and taking into account the size of the SO_4 group leads to $R_{tot}=20.5\pm 1.0$ Å. Note that the condition of Eq. (13) implies $R_{tot}\geqslant 19.0$ Å for the assumed R_{eff} value.

The fully extended chain represents a maximum value for R_{par}. As discussed previously [5], there are reasons to prefer this value to shorter ones in the case of spheres and cylinders, as the geometrical packing constraints are relaxed only in the case of lamellar structures, and the disordered bilayer shrinks considerably. However, small contractions, especially at high temperatures, cannot be excluded, so this R_{par} represents an upper limit.

It is well known that the sulfate groups remain linked to the micelle surface together with hydration water and a fraction of counterions. In our case, a layer of thickness 4.6 Å [21] around R_{eff} is enough to accommodate all SO_4^- groups plus four water molecules per head in the cylindrical part of the micelle. In the spherical end caps the amount of water is larger, possibly doubled. The fraction of counterions within the polar shell is not an important parameter in ρ_{pol} because the Na^+ counterion is not sensitive enough to x ray and its electron density can be easily masked by water replacement. The obtained ρ_{pol} values around 0.45–0.50 e/A^3 are in agreement with those used by modeling [15,16].

From the obtained R values, Eq. (13) gives 170 and 640 Å as lower and upper limits for L, as function essentially of the imprecision in R_{tot}. A value $L=260$ Å corresponds to $R_{tot}=20.5$ Å, which shows how critical is the L value obtained as a function of the R_{tot} value adopted. As a function of such criticality, a more defined determination of L from the diffraction data could be done if R_{tot} is known with better precision from other techniques.

It is to be noted that smaller values for R_{par} and/or smaller polar head thickness would lead to even larger micellar sizes. In the case of SLS the 1/3 behavior, which defines water separation in the three dimensions, may be due more to the rigidity of the micelles than to their small sizes. The actual micellar size should be checked by other experimental techniques. Previous NMR results on this system [24] implied long micelles and are in agreement with the upper limit of the present interpretation of data that also takes into account crystallographic arguments related to H_α phases [25].

It may be concluded that micellar growth in the SLS-water system occurs at the I-H transition, a behavior expected in statistical mechanical models [7] for small sizes in the isotropic phase.

The present analysis suggests a comment about the previously investigated systems [10]. In particular, it should be stressed that H phases with different structural properties

could exist. In those systems in which the relationship $L/C=1$ does not occur and Eq. (3) is not verified, the analysis of the a vs c_ν behavior should take into account flexibility-rigidity of the micelles as well as their size and capacity to grow. In the case of flexible-finite rods, the analysis is particularly delicate, as theories have not been derived yet. Another aspect concerns the micellar radius: the formalism now developed allows a more detailed analysis of the results in terms of micellar size. The strong dependence of the particle length on the particle radius considered is relaxed through the variable amount of bound water defining $R_{\rm tot}$.

It is worthwhile to point out that these results evidencing finite rods in the H phase have as analog the growing evidence shaking also the picture of infinite lamellae in the lamellar L phase. Besides growing experimental evidence for disruptions-pores in the membranes [26,27], the theoretical models for self-association indicate the possibility of finite planar aggregates [7] and also rim curved defects [28,29].

ACKNOWLEDGMENTS

Thanks are due to CNPq (Brazil) and CNR (Italy) for financial support. We acknowledge the collaboration of A. Gulik in forwarding the measured diffraction intensities.

[1] V. Luzzati, H. Mustacchi, A. Skoulios, and F. Husson, Acta Crystallogr. **13**, 660 (1960); F. Husson, H. Mustacchi, and V. Luzzati, *ibid*. **13**, 668 (1960); V. Luzzati, in *Biological Membranes*, edited by D. Chapman (Academic, New York, 1968), p. 71.
[2] J. M. Seddon, Biochim. Biophys. Acta **1031**, 1 (1990).
[3] R. Hentschke and J. Herzfeld, Phys. Rev. A **44**, 1148 (1991).
[4] L. Q. Amaral, R. Itri, P. Mariani, and R. Micheletto, Liq. Cryst. **12**, 913 (1992).
[5] L. Q. Amaral, A. Gulik, R. Itri, and P. Mariani, Phys. Rev. A **46**, 3548 (1992).
[6] R. Hentschke, M. P. Taylor, and J. Herzfeld, Phys. Rev. A **40**, 1678 (1989); Phys. Rev. Lett. **62**, 800 (1989).
[7] M. P. Taylor and J. Herzfeld, Phys. Rev. A **43**, 1892 (1991).
[8] T. J. Sluckin, Liq. Cryst. **6**, 111 (1989).
[9] P. Mariani and L. Q. Amaral, Phys. Rev. E **50**, 1678 (1994).
[10] P. Mariani, L. Q. Amaral, L. Saturni, and H. Delacroix, J. Phys. (France) II **4**, 1393 (1994).
[11] H. Franz, F. Ciuchi, G. di Nicola, M. M. de Morais, and P. Mariani, Phys. Rev. E **50**, 395 (1994); F. Ciuchi, G. di Nicola, H. Franz, G. Gottarelli, P. Mariani, M. G. Bossi, and G. P. Spada, J. Am. Chem. Soc. **116**, 7064 (1994).
[12] R. Itri, C. V. Teixeira, and L. Q. Amaral (unpublished).
[13] R. Itri and L. Q. Amaral, J. Phys. Chem. **95**, 423 (1991).
[14] R. Itri and L. Q. Amaral, J. Appl. Crystallogr. **27**, 20 (1994).
[15] R. Itri and L. Q. Amaral, J. Phys. Chem. **94**, 2198 (1990).
[16] R. Itri and L. Q. Amaral, Phys. Rev. E **47**, 2551 (1993).
[17] A. Tardieu, Ph.D. thesis, Université Paris Sud, 1972.
[18] N. P. Franks, J. Mol. Biol. **100**, 345 (1976).
[19] A. E. Blauroch, J. Mol. Biol. **56**, 35 (1971).
[20] P. Mariani, V. Luzzati, and H. Delacroix, J. Mol. Biol. **204**, 165 (1988).
[21] D. Stigter, J. Phys. Chem. **68**, 3603 (1964).
[22] C. Tanford, J. Phys. Chem. **76**, 3020 (1972).
[23] F. Reis Husson, J. Mol. Biol. **25**, 363 (1967).
[24] P. O. Quist, B. Halle, and I. Furo, J. Chem. Phys. **95**, 6945 (1991).
[25] V. Luzzati, J. Phys. (France) II **5**, 1649 (1995).
[26] M. C. Holmes and J. Charvolin, J. Phys. Chem. **88**, 810 (1984).
[27] P. O. Quist, K. Fontell, and B. Halle, Liq. Cryst. **16**, 235 (1994).
[28] C. K. Bagdassarian, D. Roux, A. Ben-Shaul, and W. M. Gelbart, J. Chem. Phys. **94**, 3030 (1991).
[29] R. Granek, W. M. Gelbart, Y. Bohbot, and A. Ben-Shaul, J. Chem. Phys. **101**, 4331 (1994).